Dalton Transactions

Accepted Manuscript

ROYAL SOCIETY OF CHEMISTRY

www.rsc.org/dalton

A highly efficient binder for the selective recognition and determination of $Hg(NO_3)_2$ concentrations in kidney and liver tissues of a fish using fluorescence method is described.

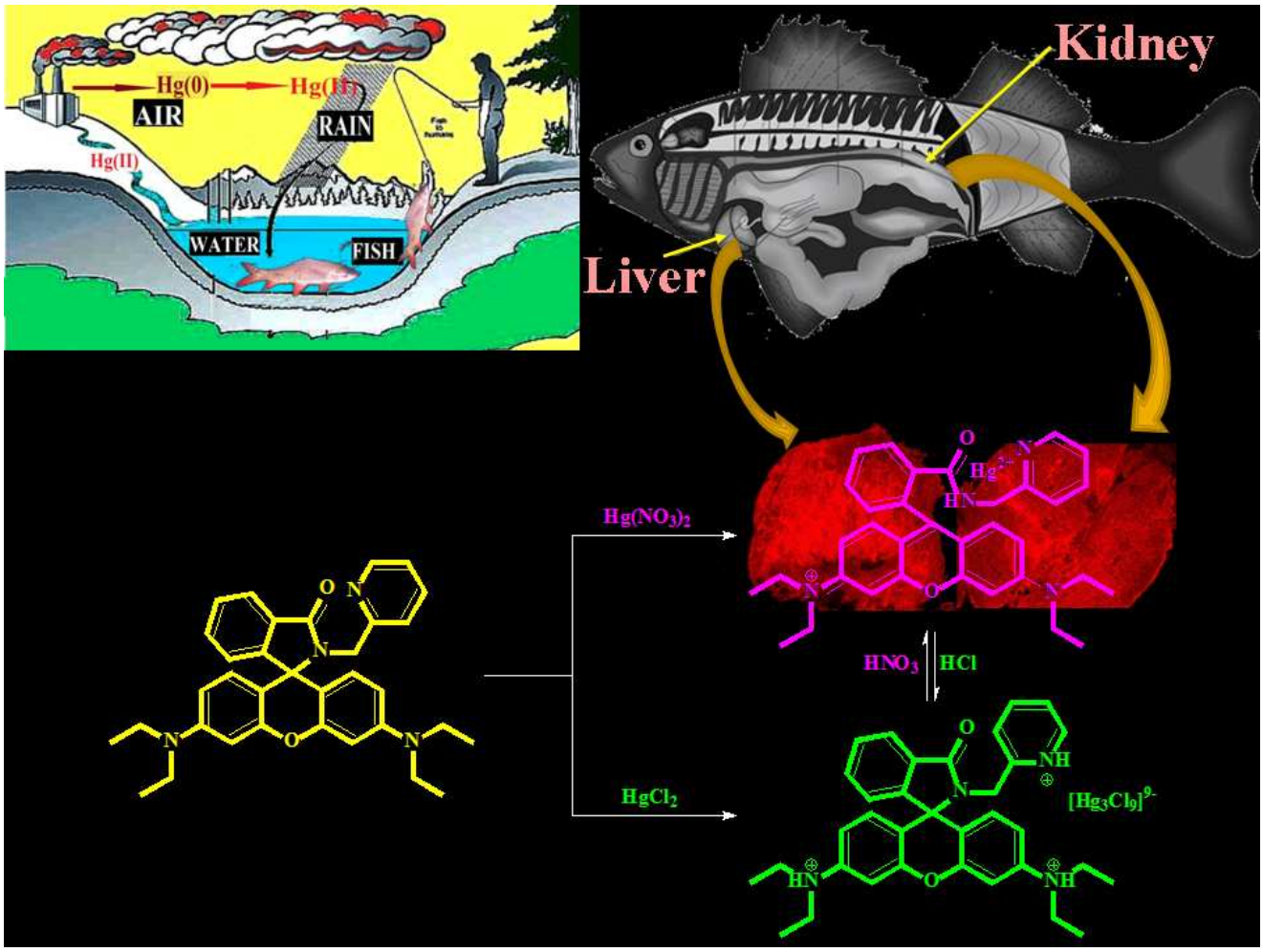

Cite this: DOI: 10.1039/c0xx00000x

www.rsc.org/xxxxxx

ARTICLE TYPE

Anion induced multisignaling probe for Hg^{2+} and its application for fish kidney and liver tissue imaging studies

Sandip Mandal,[a] Arnab Banerjee,*[a] Debasree Ghosh,[b] Dipak Kumar Mandal,[b] Damir A. Safin,*[c] Maria G. Babashkina,[c] Koen Robeyns,[c] Mariusz P. Mitoraj,*[d] Piotr Kubisiak,[d] Yann Garcia[c] and Debasis Das*[a]

Received (in XXX, XXX) Xth XXXXXXXXX 20XX, Accepted Xth XXXXXXXXX 20XX
DOI: 10.1039/b000000x

3',6'-Bis(diethylamino)-2-(pyridin-2-ylmethyl)spiro[isoindoline-1,9'-xanthen]-3-one (**L**) was synthesized for the selective fluorescence and colorimetric recognition of Hg^{2+} at pH 6.0. In addition, **L** was useful for imaging Hg^{2+} in fish kidney and liver tissue using a fluorescence microscope. Spirolactam ring opening of **L** for Hg^{2+} recognition is strongly influenced by the nature of the mercury salt and found to be NO_3^--induced. Other mercury salts such as $HgCl_2$, $Hg(CH_3COO)_2$ and $Hg(ClO_4)_2$ failed to induce fluorescence and colorimetric response of **L** under the same experimental conditions. For instance, the former salt does not exhibit spirolactam ring opening but forms a new ionic compound $(H_3L)_2[Hg_6Cl_{18}]\cdot 2H_2O$ (**1**), which structure has been elucidated by single crystal X-ray diffraction. This might be explained by 1) the higher covalent nature of Hg^{2+} and, hence, for the lower acidity of the metal center and its inability to induce the ring opening reaction, and 2) bulky anion, in the case of $Hg(ClO_4)_2$, which is also ionic, leading to steric hindrance to accommodate within the $N(Et)_2$ group upon spirolactam ring opening.

Introduction

Mercury, a well-known toxic metal, causes strong damage to the central nervous system, various cognitive and motor disorders, and Minamata disease.[1] United States Environmental Protection Agency (USEPA)[2] recommends 0.002 mg L^{-1} as a maximum mercury tolerance level in drinking water.

Several techniques such as. spectrophotometry,[3] atomic absorption spectrometry,[4] inductively coupled plasma-atomic emission spectrometry[5] and voltammetry[6] are available for the determination of mercury traces. However, most of these techniques require sophisticated and costly instruments associated with complicated operational procedures. Fluorescence detection of Hg^{2+}, being widely used in biological, toxicological and environmental studies, offers significant advantages over other methods, *e.g.* non-destructive nature, high sensitivity, and instantaneous response.[7] Recently, we have developed several sensors for cations,[8] including some for Hg^{2+}.[9]

Fish seems to be the most important source of Hg^{2+} in a human body,[10] and, thus, determination of Hg^{2+} in different organs of a fish is vital. Although plenty of Hg^{2+} selective fluorescence probes have been reported,[11] their use for the trace level determination of Hg^{2+} in various fish organs is rare. For this purpose, we have studied *Labeo rohita* (Hamilton), a freshwater indian major carps, which is a rich source of protein for human beings having a high commercial demand on the market.[12]

Visible light excitable fluorescence probe is highly demanding for biological studies as it minimizes the sample damage and native auto-fluorescence events, associated with ultraviolet excitation. Rhodamine derived probes have a long wavelength absorption and emission properties to provide a convenient platform for colorimetric "naked eye" and/or fluorescence recognition *via* spirolactam ring opening.[13]

Recently, interaction of a quinoline containing rhodamine 6G derivative with different Hg^{2+} salts such as $HgCl_2$, HgI_2, $Hg(NO_3)_2$ and $Hg(ClO_4)_2$ was reported.[14] Among them only nitrate and perchlorate salts induce spirolactam ring opening and, hence, allow their colorimetric and flurescence recognition.[14] The present probe was found to be a dual sensor that undergo fluorescence enhancement in presence of both Hg^{2+} and Cr^{3+}. However, we have directed and confined our attention to 3',6'-bis(diethylamino)-2-(pyridin-2-ylmethyl)spiro[isoindoline-1,9'-xanthen]-3-one (**L**)[15] as a possible Hg^{2+} sensor and performed comprehensive studies on the influence of the nature of mercury salt for spirolactam ring opening in **L**.

Results and discussion

Although compound **L** was reported recently,[15] we have applied new synthetic approach (Scheme 1), allowing to avoid using highly toxic phosphoryl chloride.

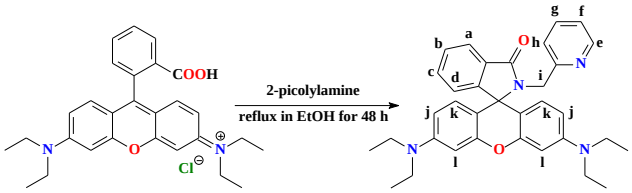

Scheme 1

The UV/vis spectrum of **L** exhibits an absorbtion band centered at 545 nm, which is characteristic for the closed spirolactam ring (Fig. 1). In the presence of $Hg(NO_3)_2$, the band is red-shifted to 555 nm with the appearance of pink color (Fig. 1). $HgCl_2$ and $Hg(CH_3COO)_2$ failed to change the color. Thus, **L** is useful for the naked eye detection of $Hg(NO_3)_2$ in the presence of different cations (Fig. 2).

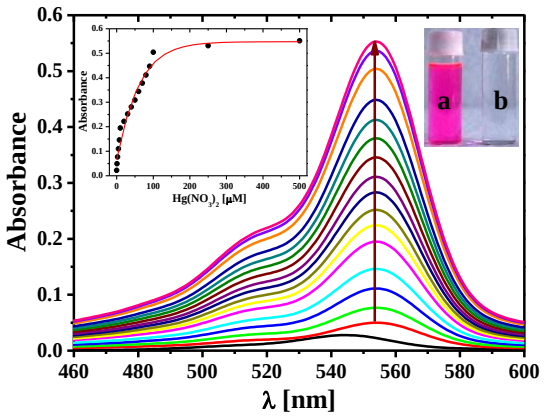

Fig. 1 Changes of the UV/vis spectra of the **L** solution (10 μM, DMSO–H_2O (3:7, v/v), 0.1 M HEPES buffer, pH 6.0) with the externally added $Hg(NO_3)_2$ (1.0, 2.5, 7.5, 10, 20, 30, 40, 50, 60, 70, 80, 90, 100, 250, 500 μM). The left inset shows the plot of absorbance of **L** (10 μM, DMSO–H_2O (3:7, v/v), 0.1 M HEPES buffer, pH 6.0) at 555 nm as a function of the externally added $Hg(NO_3)_2$ (1–500 μM). The right inset shows the naked eye color of **L** (10 μM, DMSO–H_2O (3:7, v/v), 0.1 M HEPES buffer, pH 6.0) with the externally added $Hg(NO_3)_2$ (500 μM) (a), and free **L** (10 μM) (b).

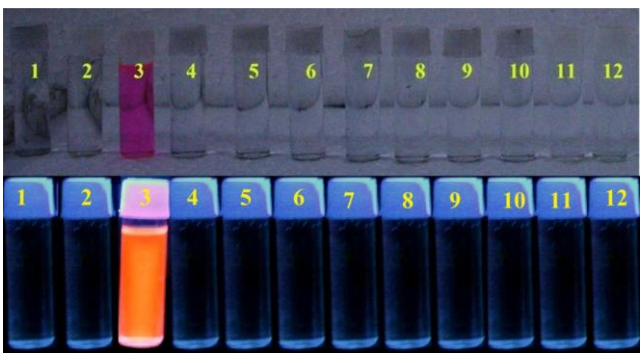

Fig. 2 Naked eye (top) and UV light irradiated (bottom) color of **L** (10 μM, DMSO–H_2O (3:7, v/v), 0.1 M HEPES buffer, pH 6.0) in the presence of different metal nitrates (500 μM): free **L** (1) Fe^{3+} (2), Hg^{2+} (3), Mn^{2+} (4), Mg^{2+} (5), Cd^{2+} (6), Cu^{2+} (7), Pb^{2+} (8), Co^{2+} (9), Ni^{2+} (10), Ag^{+} (11) and Zn^{2+} (12).

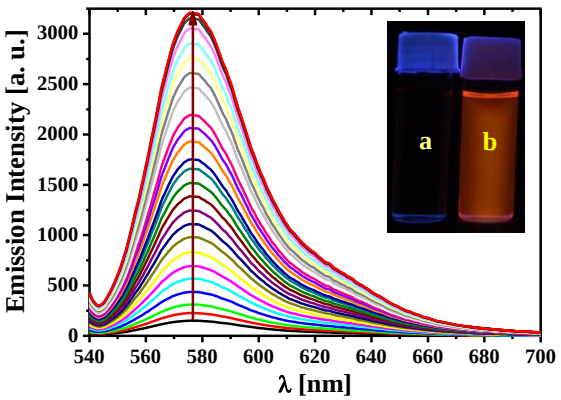

Fig. 3 Changes of the emission spectra of the **L** solution (1 μM, DMSO–H_2O (3:7, v/v), 0.1 M HEPES buffer, pH 6.0, λ_{ex} = 540 nm) with the externally added $Hg(NO_3)_2$ (0.1, 0.25, 0.75, 1, 2, 3, 4, 5, 6, 7, 8, 9, 10, 25, 50, 100 μM). The inset shows UV light irradiated color of the free **L** (1 μM) (a), and **L** (1 μM, DMSO–H_2O (3:7, v/v), 0.1 M HEPES buffer, pH 6.0) with the externally added $Hg(NO_3)_2$ (100 μM) (b).

It was found that **L** exhibits very weak fluorescence at 575 nm (Φ = 0.05). Gradual addition of $Hg(NO_3)_2$ leads to maximum of ~22 fold fluorescence enhancement (Φ = 0.25) (Fig. 3). The plot of the emission intensity *vs.* $Hg(NO_3)_2$ concentration generates a sigmoidal graph with the linear region up to 10 μM of $Hg(NO_3)_2$ (Fig. 4), which is useful to determine the concentration of $Hg(NO_3)_2$. No significant changes of the fluorescence intensity of **L** have been observed in the presence of 100 equivalents of common cations (Fig. 5).

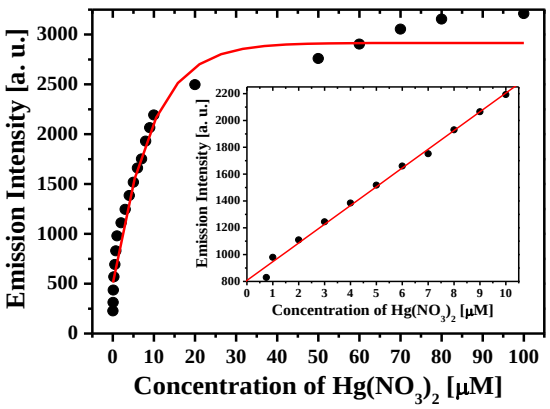

Fig. 4 Emission intensity of the **L** solution (1 μM, DMSO–H_2O (3:7, v/v), 0.1 M HEPES buffer, pH 6.0, λ_{ex} = 540 nm) at 575 nm *vs.* externally added $Hg(NO_3)_2$.

In the presence of $Hg(NO_3)_2$, emission intensity of **L** becomes maximum in the pH range of 5.0–9.0 (Fig. 6). It should be noted, that a higher mercury concentration was found in fish grown from lakes having pH 6.0–6.5 or less,[16] and hence, all experiments have been performed at pH 6.0.

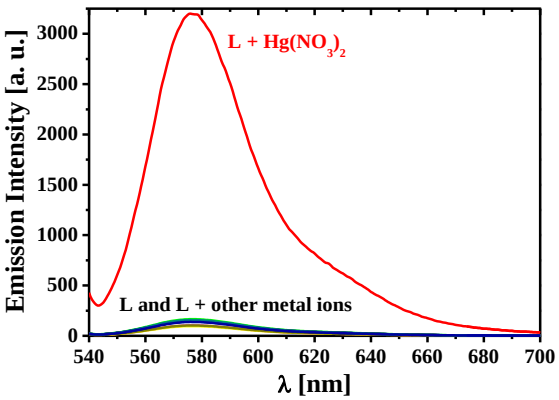

Fig. 5 Emission spectra of the **L** solution (1 μM, DMSO–H_2O (3:7, v/v), 0.1 M HEPES buffer, pH 6.0, λ_{ex} = 540 nm) with the externally added nitrate salts of Na^+, K^+, Mg^{2+}, Ca^{2+}, Cr^{3+}, Mn^{2+}, Fe^{3+}, Co^{2+}, Ni^{2+}, Cu^{2+}, Zn^{2+}, Ag^+, Cd^{2+} and Hg^{2+} (100 μM).

Interestingly, only $Hg(NO_3)_2$ can enhance emission intensity of **L**, while other mercury salts such as $HgCl_2$, $Hg(CH_3COO)_2$ and $Hg(ClO_4)_2$ failed (Fig. 7). The proposed interaction mechanism of **L** with $Hg(NO_3)_2$ at pH 6.0, leading to spirolactam ring opening of the rhodamine unit, with "turn-on" fluorescence is shown in Fig. 8.

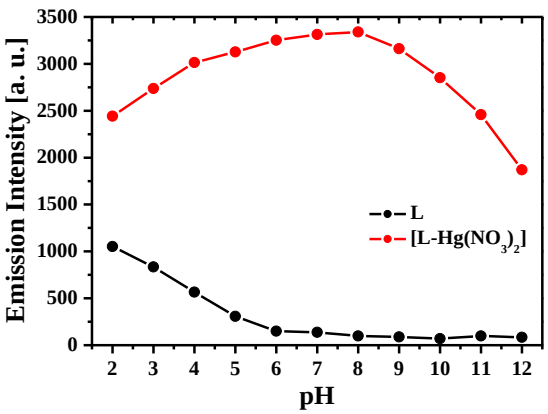

Fig. 6 Effect of pH on the emission intensities of the **L** solution (1 μM, DMSO–H_2O (3:7, v/v), 0.1 M HEPES buffer, pH 6.0, λ_{ex} = 540 nm, λ_{em} = 575 nm) and with the externally added $Hg(NO_3)_2$ (100 μM).

In the case of $HgCl_2$, an ionic interaction between two triply protonated $(H_3\mathbf{L})^{3+}$ cations and an oligomeric $[Hg_6Cl_{18}]^{6-}$ anion has been observed. Thus, the formation of $(H_3\mathbf{L})_2[Hg_6Cl_{18}]\cdot 2H_2O$ (**1**) was found (Fig. 9, Table S1 in ESI†). Dimeric species of **1** in the crystal structure are tightly packed (Fig. 9) through the formation of intermolecular hydrogen bonds (Table S2 in ESI†).

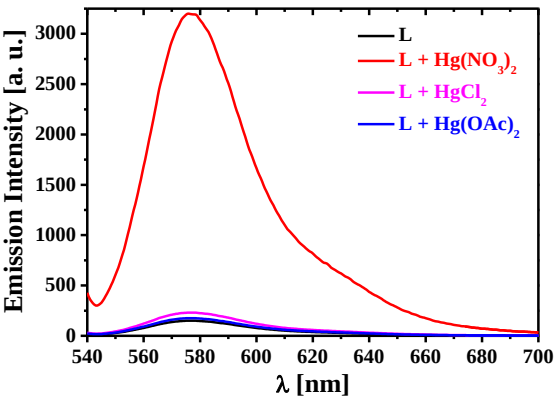

Fig. 7 Emission spectra of the **L** solution (1 μM, DMSO–H_2O (3:7, v/v), 0.1 M HEPES buffer, pH 6.0, λ_{ex} = 540 nm) with the externally added Hg^{2+} salts (100 μM).

The spirolactam ring in **1** remains intact, and, hence, no fluorescence change is observed. Thus, $HgCl_2$ does not interact with **L** but forms a new ionic compound. Similarly, in the case of $Hg(CH_3COO)_2$, Hg^{2+} failed to react with **L**. On the other hand, $Hg(NO_3)_2$, exhibiting a salt-like structure, can interact with **L** leading to spirolactam ring opening. The nitrogen atom of one of the $N(Et)_2$ functions becomes positively charged and, subsequently, the NO_3^- anion gets closer associated with the $\{N(Et)_2\}^+$ unit due to the dipole interaction. Interestingly, $Hg(ClO_4)_2$, although being ionic, cannot open the spirolactam ring of **L**. This might be due to a significantly larger size of ClO_4^- being too bulky to accommodate within the $\{N(Et)_2\}^+$ group. In case of the rhodamine 6G derivative, the NH(Et) function provides less steric repulsion towards ClO_4^- to neutralize the charge associated with $\{NH(Et)\}^+$, resulting in spirolactam ring opening.[14]

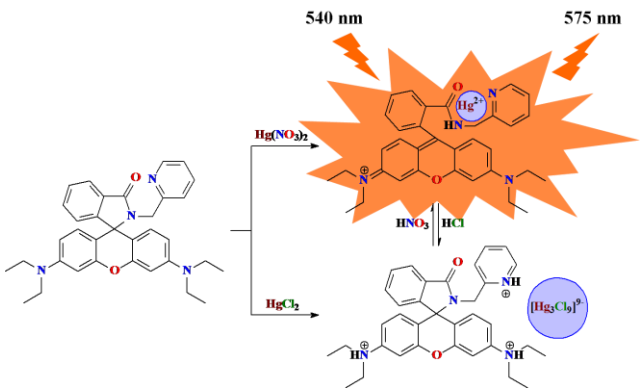

Fig. 8 The proposed sensing mechanism of $Hg(NO_3)_2$ by **L**.

Another interesting fact is that two systems [**L**–$Hg(NO_3)_2$] and [**L**–$HgCl_2$] are inter-convertable in the presence of HCl and HNO_3, respectively. The latter system, obtained from a mixture of **L** and $HgCl_2$ at pH 6.0 can also be prepared from the solution of **L**, $Hg(NO_3)_2$ and HCl at pH 6.0.

Job's plot indicates a 1:1 stoichiometry of the [**L**–$Hg(NO_3)_2$] system (Fig. 10). Binding constant of **L** with $Hg(NO_3)_2$ has been determined using the Benesi-Hildebrand equation (Fig. 11):[17] $1/\Delta F = 1/\Delta F_{max} + (1/K[C]^n) \times (1/\Delta F_{max})$. Here $\Delta F = (F_x - F_0)$ and $\Delta F_{max} = F_{lim} - F_0$, where F_0, F_x, and F_{lim} are the emission intensities of **L** in the absence of $Hg(NO_3)_2$, at an intermediate $Hg(NO_3)_2$ concentration, and at a concentration of the complete interaction, respectively. *K* is the binding constant, [C] is the concentration of $Hg(NO_3)_2$ and *n* is the number of $Hg(NO_3)_2$ bound each **L** (here $n = 1$). The value of *K* was found to be 6.68×10^7 M^{-1}. **L** can detect as low as 10 nM $Hg(NO_3)_2$ (see Experimental Section).

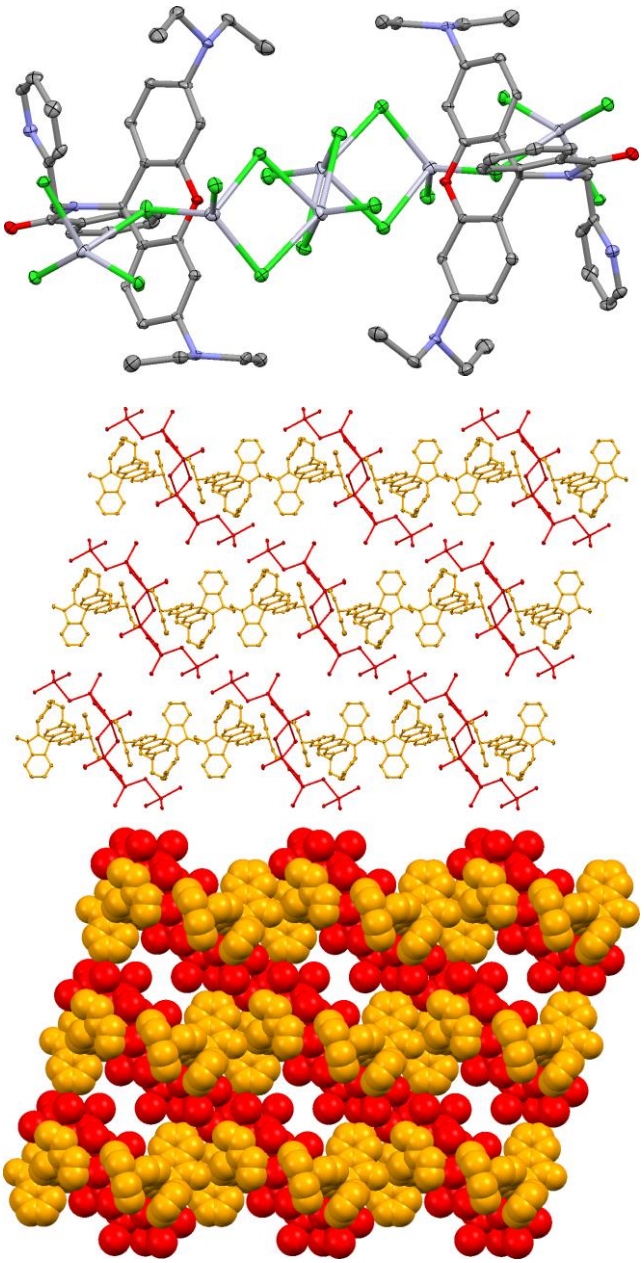

Fig. 9 Molecular structure (top; color code: C = grey, N = blue, Cl = green, Hg = light grey) and crystal packing (middle and bottom) of **1**. H-atoms and water molecules were omitted for clarity.

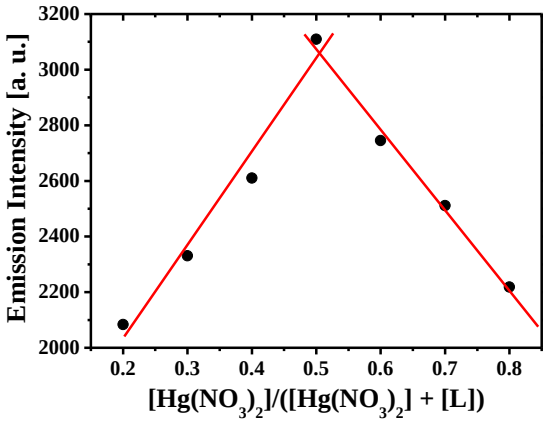

Fig. 10 Job's plot for the determination of stoichiometry of the [**L**–$Hg(NO_3)_2$] system (λ_{ex} = 540 nm, λ_{em} = 575 nm).

The fluorescence response of **L** towards $Hg(NO_3)_2$ in the presence of common cations and anions has also been studied (Fig. 12). No significant interference has been observed.

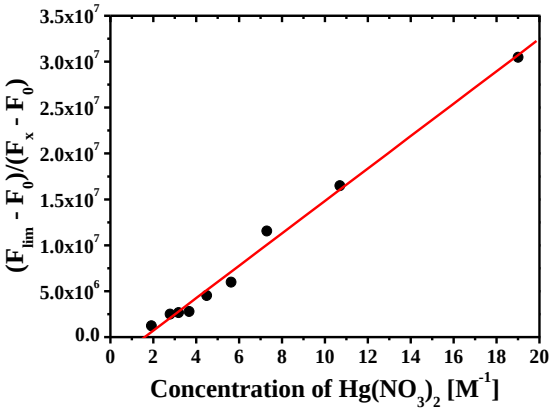

Fig. 11 Determination of the binding constant of the [**L**–$Hg(NO_3)_2$] system (λ_{ex} = 540 nm, λ_{em} = 575 nm).

The ^1H NMR titration of **L** with both $Hg(NO_3)_2$ and $HgCl_2$ further supports the proposed mechanism. In case of $Hg(NO_3)_2$ (Fig. 13), the spirolactam ring of the rhodamine unit opens as the amide NH of the ligand at 7.34 ppm have gradually lowfield shifted to 7.46 ppm, indicating the binding of amide NH to Hg^{2+}. Furthermore, remarkable lowfield shifts of the pyridine proton "e" (from 8.11 ppm to 8.42 ppm) and the CH_2 proton (from 4.23 ppm to 4.60 ppm) further support this conclusion. However, addition of $HgCl_2$ do not effect on the ^1H NMR spectrum of **L** (Fig. 13).

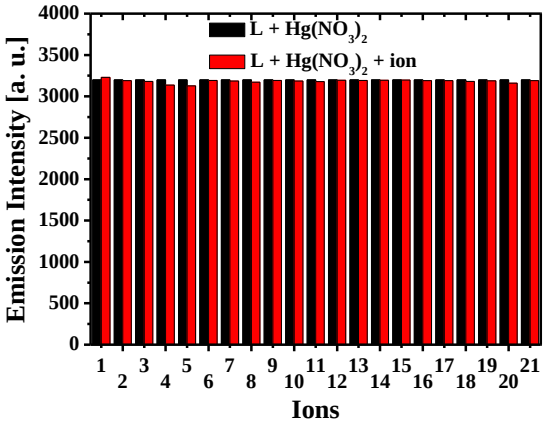

Fig. 12 Interference of different ions [Na^+ (1), K^+ (2), Ca^{2+} (3), Mg^{2+} (4), Zn^{2+} (5), Cu^{2+} (6), Pb^{2+} (7), Co^{2+} (8), Ni^{2+} (9), Fe^{3+} (10), Ag^+ (11), Cd^{2+} (12), Cr^{3+} (13), Al^{3+} (14), Mn^{2+} (15), Cl^- (16), OAc^- (17), citrate (18), lactate (19), HCO_3^- (20), $H_2PO_4^-$ (21)] on the determination of $Hg(NO_3)_2$ by **L** (DMSO–H_2O (3:7, v/v), 0.1 M HEPES buffer, pH 6.0, λ_{ex} = 540 nm, λ_{em} = 575 nm). [**L**] = 1 μM, [$Hg(NO_3)_2$] = [foreign ion] = 100 μM.

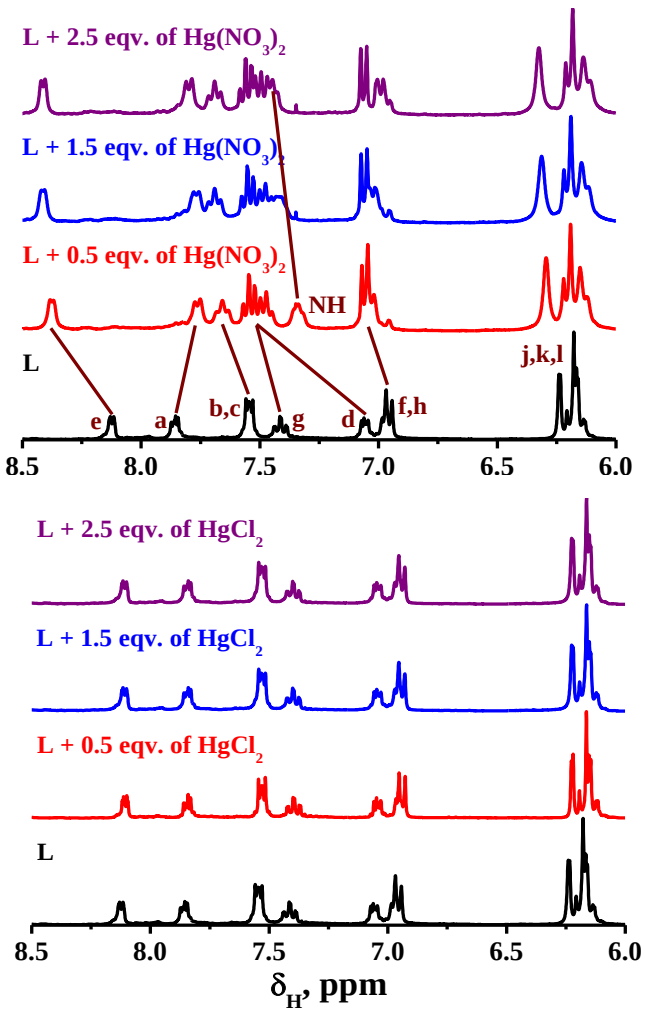

Fig. 13 ^1H NMR titration of **L** by $Hg(NO_3)_2$ (top) and $HgCl_2$ (bottom) in DMSO-d_6. For the labelling of peaks see Scheme 1.

It is also established that **L** is highly efficient for the recognition and imaging of $Hg(NO_3)_2$ in the contaminated kidney and liver tissues of *Labeo rohita* (fish) after 15 days exposure to $Hg(NO_3)_2$ (Fig. 14). The obtained results are in agreement with the previously reported data.[18]

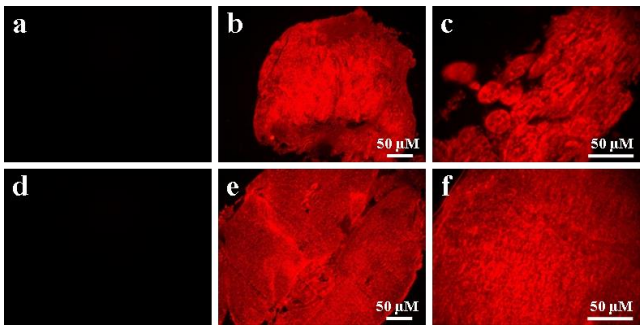

Fig. 14 Kidney (top row) and liver (bottom row) tissues of *Labeo rohita* after 15 days exposure to $Hg(NO_3)_2$ (a and d), and after staining with **L** under 100 (b and e) and 400 (c and f) magnification, respectively.

In order to shed some light on the possible structure of **L** and its complex with Hg^{2+}, we have performed static DFT calculations, based on the ADF program[19] with DFT/BLYP-D3/TZP as well as *ab initio* Car-Parrinello and Born-Oppenheimer molecular dynamics simulations. The former dynamics simulations have been done by means of the CPMD program,[20] whereas the latter ones are based on the CP2K package.[20d,21] In addition, calculations based on the Gaussian 09.D01 program[22] have been performed.

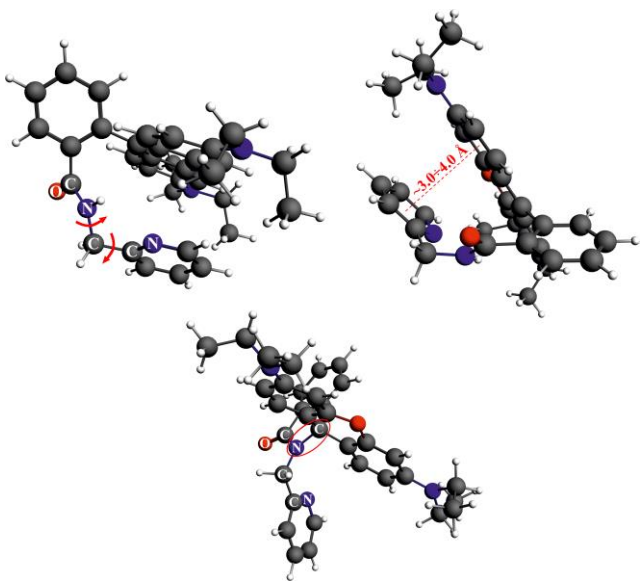

Fig. 15 The lowest energy structures of HL^+ (top) and **L** (bottom) obtained from ADF/DFT/BLYP-D3/TZP.

At first point we have determined the lowest energy conformation of **L** (Fig. 15 bottom). Due to the acidic environment applied in the experiments, we have subsequently considered various models of the protonated form $\mathbf{HL}^+$ (Fig. 15 top, and Fig. S1 and Table S3 in ESI†). It should be noted that the spirolactam ring is already opened in $\mathbf{HL}^+$ as opposed to the neutral ligand **L** (Fig. 15). Further inspection of the geometry shows that the pyridine ring is oriented parallel to the aromatic plane of the rhodamine fragment and suggests a π–π stacking interaction. The non-covalent interaction analysis,[23] based on the reduced density gradient, supports this observation (Fig. S2 in ESI†). Furthermore, when the geometry optimization is performed without a dispersion correction, these two rings are not stacked anymore. In order to include the entropic factors and describe possible conformations of $\mathbf{HL}^+$ in more realistic conditions, we have also run *ab initio* Car-Parrinello molecular dynamics simulations by considering the temperature value 298.15 K. The results are in line with the static DFT calculations and demonstrate that most of the time the pyridine ring is interacting with the rhodamine plane through a π–π stacking interaction (animation HL.mpg in ESI†).

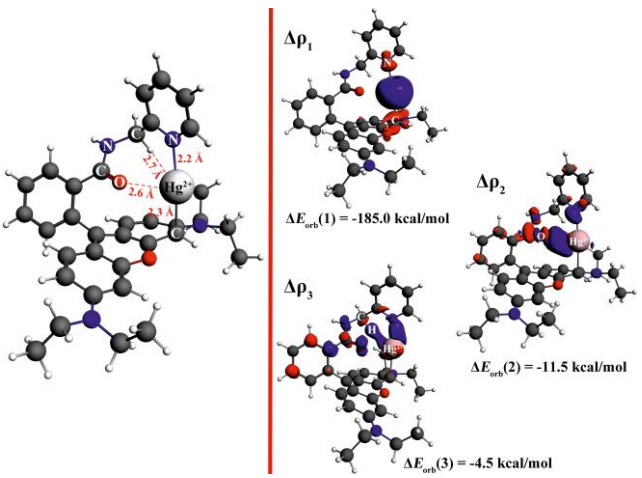

Fig. 16 The lowest energy structure of [$\mathbf{HL}^+$–Hg^{2+}] (left) and the NOCV-based deformation density channels $\Delta\rho_1$, $\Delta\rho_2$, $\Delta\rho_3$, depicted with the corresponding energies, $\Delta E_{orb}(1)$, $\Delta E_{orb}(2)$, $\Delta E_{orb}(3)$, describing the specific bonding contributions (right). Red color of $\Delta\rho_i$ shows the charge depletion, whereas blue color demonstrates the electron density accumulation due to the formation of bonds with Hg^{2+}.

The ground state structure of **L** (Fig. 16 left) as well as CPMD trajectory (animation HL.mpg in ESI†) suggest a possible conformational flexibility of the system arising from rotations around the CH_2–N and/or CH_2–C(Py) bonds. When Hg^{2+} is present in solution it is likely that it will be captured by both the rhodamine plane and the $PhC(O)NHCH_2Py$ fragment. It is indeed the case as it can be seen from the lowest energy conformation of the [$\mathbf{HL}^+$–Hg^{2+}] complex obtained from the static DFT calculations (Fig. 16 left). The CP2K molecular dynamics simulations at 298.15 K further points the same lowest energy structure (animation HL-Hg.mpg in ESI†). The ETS-NOCV bonding analysis demonstrates that Hg^{2+} is strongly bound to the nitrogen center of the pyridine ring as well as to the rhodamine plane as suggested by the contour $\Delta\rho_1$ and the corresponding $\Delta E_{orb}(1)$ = –185.0 kcal/mol (Fig. 16 right). The second, less important bonding contribution, characterized by the channel $\Delta\rho_2$ and the corresponding stabilization energy $\Delta E_{orb}(2)$ = –11.5 kcal/mol, stems from the interaction of Hg^{2+} with the oxygen center. Finally, one can also notice the agostic interaction $\Delta\rho_3$, formed between the C–H bond and Hg^{2+} (Fig. 16 right), which leads to weak stabilization energy $\Delta E_{orb}(3)$ = –4.5 kcal/mol. The existence of the interaction between Hg^{2+} and pyridine ring and CH_2 unit is consistent with the low-field signals of the protons observed in the ^{1}H NMR spectrum (Fig. 13). The structure of [$\mathbf{HL}^+$–Hg^{2+}] suggests that the fluorescence enhancement can be due to the chelation enhancement process (CHEF). It should be noted that in $Hg(NO_3)_3$, the bond energy, describing the interaction between Hg^{2+} and NO_3^- is the weakest compared to $HgCl_2$ and $Hg(OAC)_2$ (Table S4 in ESI†). This qualitatively explains the observed fluorescence enhancement in the former case.

In order to obtain a qualitative picture of the absorption spectra, we have performed a TD-DFT/B3LYP/TZP study with inclusion of solvent effects at the COSMO level as implemented in the ADF program for both $\mathbf{HL}^+$ and [$\mathbf{HL}^+$–Hg^{2+}]. The dominant absorption band of $\mathbf{HL}^+$ (f = 0.75 a. u.) is observed at 550 nm (Fig. 17). It is in good agreement with the experimental value of 545 nm. Decomposition of this transition into the molecular orbitals shows that absorption is of the type $\pi \rightarrow \pi^*$ and it engages predominantly the HOMO and LUMO molecular orbitals located at the rhodamine rings. A similar qualitative picture of absorption is observed for [$\mathbf{HL}^+$–Hg^{2+}]: the maximum peak at 515 nm involves solely the HOMO → LUMO transition (Fig. S4 in ESI†). The most evident difference between the absorption spectra of $\mathbf{HL}^+$ and [$\mathbf{HL}^+$–Hg^{2+}] appeared to be the oscillator strength, which is significantly higher in the latter case (f = 0.75 a. u. for $\mathbf{HL}^+$ and f = 1.18 a. u for [$\mathbf{HL}^+$–Hg^{2+}]. This is fully consistent with the experimental observations (Fig. 1).

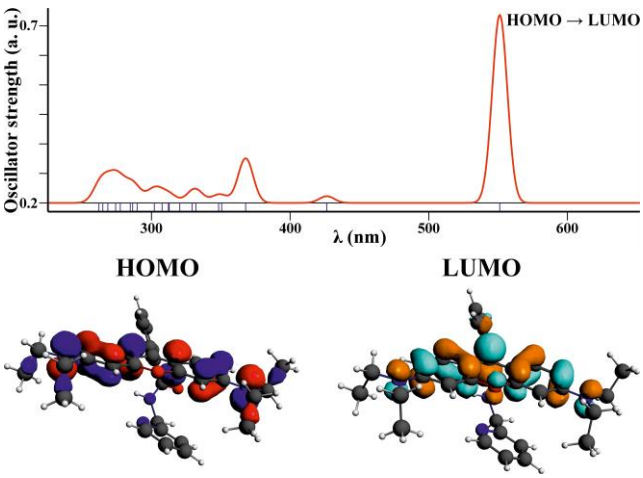

Fig. 17 The simulated TD-DFT/B3LYP/TZP spectrum of $\mathbf{HL}^+$ in water (top) together with the contours of molecular orbitals (0.03 a. u.) involved in the dominant HOMO → LUMO transition (bottom).

We have finally calculated the S_1 excited state of $\mathbf{HL}^+$ based on the Gaussian 09.D01 program.[22] It is found that the energy difference between the S_1 state and the ground state S_0 is 522 nm which slightly differs from the experimental weak emission band found at 575 nm (Fig. S4 in ESI†). Lack of quantitative agreement with experiments can be related to various factors including omission of solvent effects as well as to consideration of the simplified model of **L**.

Conclusions

In summary, a new approach for the synthesis of 3',6'-bis(diethylamino)-2-(pyridin-2-ylmethyl)spiro[isoindoline-1,9'-xanthen]-3-one (**L**) has been reported. Fluorescence properties of **L** in the presence of different mercury salts have been investigated. It is established that only $Hg(NO_3)_2$ can open the spirolactam ring of **L** with significant fluorescence enhancement. Moreover, **L** is highly efficient for the recognition and determination of $Hg(NO_3)_2$ concentrations in the kidney and liver tissues of a fish using fluorescence techniques. The extensive static DFT and *ab initio* molecular dynamics simulations are applied to characterize possible structures of **L**, $\mathbf{HL}^+$ and [$\mathbf{HL}^+$–Hg^{2+}] as well as their spectroscopic properties.

Experimental

Materials

Rhodamine B and 2-picolylamine have been purchased from Sigma Aldrich (India). Spectroscopic grade solvents have been used. Either Na^+ or K^+ salts of anions, and NO_3^- or Cl^- salts of cations were used. Other chemicals are of analytical reagent grade and used without further purification. Mili-Q 18.2 MΩ cm^{-1} water has been used throughout all the experiments.

Physical measurements

FTIR spectra were recorded on a Perkin-Elmer FTIR-RX1 spectrometer. ^{1}H NMR spectra in DMSO-d_6 were recorded with a Bruker Avance 300 MHz using tetramethylsilane as an internal standard. Absorption spectra were recorded with a Shimadzu UV-2450 spectrophotometer. Steady-state fluorescence spectra were recorded with a Hitachi F-4500 spectrofluorimeter. Electrospray ionization mass spectra were recorded on a QTOF Micro YA 263 mass spectrometer. The measurement of pH was carried out on a Systronics digital pH meter (model 335, India). Elemental analyses were performed on a Perkin Elmer CHN analyzer.

Imaging system

The imaging system was composed of an inverted fluorescence microscope Leica DM 1000 LED, digital compact camera Leica DFC 420C, and an image processor Leica Application Suite v3.3.0. The microscope was equipped with a 50 W mercury arc lamp.

UV-vis and fluorescence titration

For UV-vis and fluorescence titrations a stock solution of **L** (10 μM) was prepared in DMSO:H_2O (v/v 4:1, pH 7.4). Working solutions of **L** and $Hg(NO_3)_2$ were prepared from their respective stock solutions. Fluorescence measurements were performed using a 2.5 nm × 2.5 nm slit width. All absorbtion and fluorescence spectra were recorded after 15 min of mixing of **L** with $Hg(NO_3)_2$.

Quantum yield measurements

The fluorescence quantum yields were determined using Rhodamine B as a reference with a known ϕ_{ref} value of 0.65 in basic EtOH.[24] The area of the emission spectrum was integrated using the software available in the instrument and the quantum yield was calculated according to the following equation:[25]

$$\phi_{sample} = \phi_{ref} \times [A_{sample}/A_{ref}] \times [OD_{ref}/OD_{sample}] \times [(\eta_{sample})^2/(\eta_{ref})^2],$$

where ϕ_{sample} and ϕ_{ref} were the fluorescence quantum yield of the sample and reference, respectively; A_{sample} and A_{ref} were the area under the fluorescence spectra of the sample and the reference, respectively; OD_{sample} and OD_{ref} were the corresponding optical densities of the sample and the reference solution at the wavelength of excitation; η_{sample} and η_{ref} were the refractive index of the sample and reference, respectively.

Detection limit

Fluorescence titration of **L** with $Hg(NO_3)_2$ was carried out by adding aliquots of the μM concentration of $Hg(NO_3)_2$ to **L**. The detection limit was obtained as the concentration, at which a sharp change in the emission intensity occurred, multiplied by the concentration of **L**:[26] DL = $C_L \times C_T$, where C_L was the concentration of **L**, C_T was the concentration of $Hg(NO_3)_2$ at which fluorescence enhanced. Thus, DL = 1 μM × 0.01 μM = 0.01 μM = 10 nM.

$Hg(NO_3)_2$ exposure to fish

Ten laboratory acclimatized fish were exposed to $Hg(NO_3)_2$ (0.132 mg L^{-1}, 1/5 of the LC_{50} value) for 15 days in the 50 L capacity aquarium at pH 6.0. They were kept aerated 24 h and fed with commercial feeds. Water was replaced every two days.

Tissue collection and processing

$Hg(NO_3)_2$ exposed fish were sacrificed to collect their kidney and liver tissues, washed in distilled water, fixed in 4% paraformaldehyde for 48 h, dehydrated through graded ethanol series, cleared in xylene and infiltered with the paraffin wax (56–58 °C) to obtain paraffin embedded tissue blocks. Tissues were sectioned serially having thickness of 8 μm, and spread over glass slides.

Staining with L

Slides were deparaffinized in xylene, hydrated through graded

series of ethanol, equilibrated with 2% DMSO, incubated with **L** (in 2% DMSO) for 2 min, washed several times with 2% DMSO and observed under the fluorescence microscope.

Fish assays

Omni trace ultra grade nitric acid (EM Science) was used for digestion experiments. All glassware were rinsed with dilute nitric acid and milipore water before utilization. Microwave digestions were carried out using a CEM Discover Labmate microwave synthesizer. Samples of fish tissue (100–200 mg) were dissected from frozen whole specimens after scale removal and digested in nitric acid (200–500 μL) at 180 °C upon 300W microwave irradiation for 5–10 min. The resulting solutions were neutralized with 10 N NaOH and HEPES buffer. An appropriate concentration of **L** (in HEPES buffer, pH 6.0) was used to measure the $Hg(NO_3)_2$ concentration in samples.

Density Functional Theory (DFT) based calculations

We applied in the ADF/DFT ground state optimizations, the BLYP-D3/TZP protocol. For the TD-DFT excited state optimization (S_1) of $\mathbf{HL}^+$ the B3LYP, as implemented in the Gaussian 09 package, was applied. Similarly, the absorption spectra from ADF were generated based on B3LYP/TZP. Deformation density contributions of the ETS-NOCV method were plotted based on the ADF-GUI interface.[27]

Dynamics simulations

Born-Oppenheimer Molecular Dynamics simulations were performed using the CP2K 2.5 package (Pade functional with Grimme's dispersion correction and DZVP basis sets). Calculations were conducted in NVT ensemble at 298 K with 0.5 fs timestep; over 20 ps of trajectory was collected. Molecular dynamics simulations at Car-Parrinello level were done by means of the CPMD software package, using a plane wave basis set with cutoff energy of 100 Ry within a cubic cell of 16 Å in length. We used the time step length of 4.134 atu (0.1 fs) and the inertia parameter for wavefunction dynamics (fictitious electron mass) is 500 amu. The length of simulation was ~ 20 ps. The temperature of 298 K was controlled *via* the Nosé-Hoover chain thermostat. Valence electrons were treated explicitly within the DFT formalism employing the PBE exchange-correlation functional Grimme's dispersion correction, whereas for the inner electrons description, the Goedecker type pseudopotentials were used. VMD software package was used for the preparation of each animation.[20d]

ETS-NOCV bonding analysis[28]

Historically, the Natural Orbitals for Chemical Valence (NOCV) was derived from the Nalewajski-Mrozek valence theory as eigenvectors that diagonalizes the deformation density matrix. It was shown that the natural orbitals for chemical valence pairs (ψ_{-k},ψ_k) decompose the differential density $\Delta\rho$ into NOCV-contributions ($\Delta\rho_k$):

$$\Delta\rho(r) = \sum_{k=1}^{M/2} v_k[-\psi_{-k}^2(r) + \psi_k^2(r)] = \sum_{k=1}^{M/2} \Delta\rho_k(r),$$

where v_k and M stand for the NOCV eigenvalues and the number of basis functions, respectively. Visual inspection of the deformation density plots ($\Delta\rho_k$) helps to attribute symmetry and the direction of the charge flow. In addition, these pictures are enriched by providing the energetic estimations, $\Delta E_{orb}(k)$, for each $\Delta\rho_k$ within ETS-NOCV scheme. The exact formula, which links the ETS and NOCV methods, are given below after we briefly present the basic concept of ETS scheme. In this method the total bonding energy ΔE_{total} between interacting fragments, exhibiting the geometry as in the combined complex, is divided into the three components: $\Delta E_{\text{total}} = \Delta E_{\text{elstat}} + \Delta E_{\text{Pauli}} + \Delta E_{\text{orb}}$. The first term, ΔE_{elstat}, corresponds to the classical electrostatic interaction between the promoted fragments as they are brought to their positions in the final complex. The second term, ΔE_{Pauli}, accounts for the repulsive Pauli interaction between occupied orbitals on the two fragments in the combined molecule. Finally, the last stabilizing term, ΔE_{orb} represents the interactions between the occupied molecular orbitals of one fragment with the unoccupied molecular orbitals of the other fragment as well as mixing of occupied and virtual orbitals within the same fragment (inner-fragment polarization). This energy term may be linked to the electronic bonding effect coming from the formation of a chemical bond. In the combined ETS-NOCV scheme the orbital interaction term (ΔE_{orb}) is expressed in terms of NOCV's eigenvalues (v_k) as:

$$\Delta E_{orb} = \sum_k \Delta E_{orb}(k) = \sum_{k=1}^{M/2} v_k[-F_{-k,-k}^{TS} + F_{k,k}^{TS}]$$

where $F_{i,i}^{TS}$ are diagonal Kohn-Sham matrix elements defined over NOCV with respect to the transition state (TS) density (at the midpoint between density of the molecule and the sum of fragment densities). The above components ΔE_{orb}(k) provide the energetic estimation of $\Delta\rho_k$ that may be related to the importance of a particular electron flow channel for the bonding between the considered molecular fragments. ETS-NOCV analysis was done based on the Amsterdam Density Functional (ADF)[19] package in which this scheme was implemented.

Synthesis of L

A solution of 2-picolylamine (0.865 g, 8 mmol) was added to a solution of rhodamine B (0.958 g, 2 mmol) in EtOH (20 mL). The mixture was refluxed for 48 h. Then the solvent was removed in vacuum and the crude product was purified by column chromatography with *n*-hexane:EtOAc (82:18, v/v). Yield: 0.586 g (55%). QTOF-MS ES^+, *m/z* (*I*, %): $[L + H]^+$ 533.09. *Anal*. Calc. for $C_{34}H_{36}N_4O_2$ (532.69): C 76.66, H 6.81, N 10.52. Found: C 78.51, H 6.76, N 10.62%.

Synthesis of $[Hg_3Cl_9(H_3L)]\cdot 2H_2O$ (1)

A solution of $HgCl_2$ (0.049 g, 0.18 mmol; pH 6.0 maintained using HCl) in MeOH was added drop wise to a solution of **L** (0.100 g, 0.19 mmol; pH 6.0 maintained using HCl). The reaction mixture was stirred for 1 h at room temperature and

the resulting solution was kept for 3 days at room temperature while X-ray suitable colourlees crystals of **1** appeared.

X-Ray crystallography

The X-ray data of **1** were collected at 150(2) K on a Mar345 image plate detector using Mo-K_α radiation (rotation anode, multilayer mirror). The data were integrated with the CrysAlisPro software.[29] The implemented empirical absorption correction was applied. The structures were solved by direct methods using the SHELXS-97 program[30] and refined by full-matrix least squares on $|F^2|$ using SHELXL-97.[30] Non-hydrogen atoms were anisotropically refined and the hydrogen atoms were placed on calculated positions in riding mode with temperature factors fixed at 1.2 times U_{eq} of the parent atoms. Figures were generated using the program Mercury.[31] $C_{34}H_{39}N_4O_2$, $0.5(Cl_{18}Hg_6)$, $2(H_2O)$; M_r = 1492.54 g mol^{-1}, triclinic, space group *P*–1, a = 10.4157(7), b = 11.8752(10), c = 19.1618(12), α = 102.897(6), β = 96.838(5), γ = 97.923(6)°, V = 2260.5(3) Å^3, Z = 2, ρ = 2.193 g cm^{-3}, μ(Mo-Kα) = 10.734 mm^{-1}, reflections: 22134 collected, 8405 unique, R_{int} = 0.050, R_1(all) = 0.0481, wR_2(all) = 0.1039.

CCDC 891880 contains the supplementary crystallographic data. These data can be obtained free of charge via http://www.ccdc.cam.ac.uk/conts/retrieving.html, or from the Cambridge Crystallographic Data Centre, 12 Union Road, Cambridge CB2 1EZ, UK; fax: (+44) 1223-336-033; or e-mail: deposit@ccdc.cam.ac.uk.

Acknowledgements

S. Mondal and A. Banerjee are grateful to UGC and CSIR, New Delhi for fellowships. We thank WBI (Belgium) for the postdoctoral positions allocated to D. A. Safin and M. G. Babashkina. We are grateful to UGC-DAE-CSR-Kolkata for financial assistance. Assistance from CAS (UGC) program is gratefully acknowledged. M. P. Mitoraj acknowledges the financial support from the Polish Ministry of Science and Higher Education (young researchers T-subsidy). Results presented in this work were partially obtained using PL-Grid Infrastructure and resources provided by ACC Cyfronet AGH.

Notes and references

[a] *Department of Chemistry, The University of Burdwan, Burdwan, 713104, West Bengal, India. Fax: +91 342 2530452; Tel: +91 342 2533913; E-mail: ddas100in@yahoo.com*

[b] *Fish Biology Laboratory, Department of Zoology, School of Life Sciences, Visva-Bharati University, Santiniketan, 731 235, West Bengal, India*

[c] *Institute of Condensed Matter and Nanosciences, Molecules, Solids and Reactivity (IMCN/MOST), Université Catholique de Louvain, Place L. Pasteur 1, 1348 Louvain-la-Neuve, Belgium. Fax: +32(0) 1047 2330; Tel: +32(0) 1047 2831; E-mail: damir.a.safin@gmail.com*

[d] *Department of Theoretical Chemistry, Faculty of Chemistry, Jagiellonian University, R. Ingardena 3, 30-060 Cracow, Poland. Email: mitoraj@chemia.uj.edu.pl*

† Electronic Supplementary Information (ESI) available: Fig. S1–S4 and Tables S1–S4. For ESI and crystallographic data in CIF or other electronic format see DOI: 10.1039/b000000x.

1 (*a*) T. W. Clarkson, L. Magos and G. J. Myers, *New Engl. J. Med.*, 2003, **349**, 1731; (*b*) F. Di Natale, A. Lancia, A. Molino, M. Di Natale, D. Karatza and D. Musmarra, *J. Hazard. Mater.*, 2006, **132**, 220; (*c*) C. M. L. Carvalho, E.-H. Chew, S. I. Hashemy, J. Lu and A. Holmgren, *J. Biol. Chem.*, 2008, **283**, 11913.

2 EPA 816-F-09-004, May 2009.

3 M. S. Hosseini and H. Hashemi-Moghaddam, *Talanta*, 2005, **67**, 555.

4 J. L. Manzoori, M. H. Sorouraddin and A. M. H. Shabani, *J. Anal. Atom. Spectrom.*, 1998, **13**, 305.

5 A. N. Anthemidis, G. A. Zachariadis, C. E. Michos and J. A. Stratis, *Anal. Bioanal. Chem.*, 2004, **379**, 764.

6 H. Zejli, P. Sharrock, J. L. H. H. de Cisneros, I. Naranjo-Rodriguez and K. R. Temsamani, *Talanta*, 2005, **68**, 79.

7 (*a*) U. E. Spichiger-Keller, *Chemical Sensors and Biosensors for Medical and Biological Applications*, Wiley-VCH: Weinheim, Germany, 1998; (*b*) P. T. Srinivasan, T. Viraraghavan and K. S. Subramanian, *Water SA*, 1999, **25**, 47; (*c*) K. Rurack and U. Resch-Genger, *Chem. Soc. Rev.*, 2002, **31**, 116; (*d*) V. Amendola, L. Fabbrizzi, F. Forti, M. Licchelli, C. Mangano, P. Pallavicini, A. Poggi, D. Sacchi and A. Taglieti, *Coord. Chem. Rev.*, 2006, **250**, 273.

8 (*a*) A. Sahana, A. Banerjee, S. Das, S. Lohar, D. Karak, B. Sarkar, S. K. Mukhopadhyay, A. K. Mukherjee and D. Das, *Org. Biomol. Chem.*, 2011, **9**, 5523; (*b*) A. Banerjee, A. Sahana, S. Guha, S. Lohar, I. Hauli, S. K. Mukhopadhyay, J. S. Matalobos and D. Das, *Inorg. Chem.*, 2012, **51**, 5699; (*c*) A. Sahana, A. Banerjee, S. Lohar, S. Guha, S. Das, S. K. Mukhopadhyay and D. Das, *Analyst*, 2012, **137**, 3910; (*d*) S. Das, A. Sahana, A. Banerjee, S. Lohar, D. A. Safin, M. G. Babashkina, M. Bolte, Y. Garcia, I. Hauli, S. K. Mukhopadhyay and D. Das, *Dalton Trans.*, 2013, **42**, 4757.

9 (*a*) A. Banerjee, D. Karak, A. Sahana, S. Guha, S. Lohar and D. Das, *J. Hazard. Mater.*, 2011, **186**, 738; (*b*) S. Mandal, A. Banerjee, S. Lohar, A. Chattopadhyay, B. Sarkar, S. K. Mukhopadhyay, A. Sahana and D. Das, *J. Hazard. Mater.*, 2013, **261**, 198.

10 W. F. Fitzgerald, C. H. Lamborg and C. R. Hammerschmidt, *Chem. Rev.*, 2007, **107**, 641.

11 (*a*) S. Yoon, A. E. Albers, A. P. Wong and C. J. Chang, *J. Am. Chem. Soc.*, 2005, **127**, 16030; (*b*) E. M. Nolan and S. J. Lippard, *Chem. Rev.*, 2008, **108**, 3443; (*c*) J. Hatai, S. Pal, G. P. Jose and S. Bandyopadhyay, *Inorg. Chem.*, 2012, **51**, 10129; (*d*) H. N. Kim, W. X. Ren, J. S. Kim and J. Yoon, *Chem. Soc. Rev.*, 2012, **41**, 3210; (*e*) G. Sivaraman, T. Anand and D. Chellappa, *RSC Adv.*, 2012, **2**, 10605; (*f*) T. Anand, G. Sivaraman and D. Chellappa, *Spectrochim. Acta A*, 2014, **123**, 18.

12 D. Ghosh, and D. K. Mandal, *Bull. Environ. Contam. Toxicol.*, 2012, **89**, 479.

13 (*a*) G. Sivaraman, T. Anand and D. Chellappa, *Analyst*, 2012, **137**, 5881; (*b*) A. Banerjee, A. Sahana, S.; Lohar, I. Hauli, S. K. Mukhopadhyay, D. A. Safin, M. G. Babashkina, M. Bolte, Y. Garcia and D. Das, *Chem. Commun.*, 2013, **49**, 2527; (*c*) A. Sahana, A. Banerjee, S. Lohar, A. Chottapadhyay, S. K. Mukhopadhyay and D. Das, *RSC Advances*, 2013, **3**, 14044; (*d*) A. Sahana, A. Banerjee, S. Lohar, B. Sarkar, S. K. Mukhopadhyay and D. Das, *Inorg. Chem.*, 2013, **52**, 3627; (*e*) G. Sivaraman and D. Chellappa, *J. Mater. Chem. B*, 2013, **1**, 5768; (*f*) G. Sivaraman and D. Chellappa, *J. Mater. Chem. B*, 2013, **1**, 5768; (*g*) G. Sivaraman, B. Vidya and D. Chellappa, *RSC Adv.*, 2014, **14**, 30828; (*h*) G. Sivaraman, T. Anand and D. Chellappa, *ChemPlusChem*, 2014, **79**, 1761; (*i*) G. Sivaraman, V. Sathiyaraja and D. Chellappa, *J. Lumin.*, 2014, **145**, 480.

14 S. Saha, P. Mahato, U. G. Reddy, E. Suresh, A. Chakrabarty, M. Baidya, S. K. Ghosh and A. Das, *Inorg. Chem.*, 2012, **51**, 336.

15 J. Huang, Y. Xu and X. Qian, *Dalton Trans.*, 2014, **43**, 5983.

16 D. J. Spry and J. G. Wiener, *Environ. Pollut.*, 1991, **71**, 243.

17 (*a*) H. A. Benesi and J. H. Hildebrand, *J. Am. Chem. Soc.*, 1949, **71**, 2703; (*b*) A. Banerjee, A. Sahana, S. Das, S. Lohar, S. Guha, B. Sarkar, S. K. Mukhopadhyay, A. K. Mukherjee and D. Das, *Analyst*, 2012, **137**, 2166.

18 (*a*) D. Ghosh and D. K. Mandal, *Bull. Environ. Contam. Toxicol.*, 2012, **89**, 479; (*b*) D. Ghosh and D. K. Mandal, *Asian J. Exp. Biol. Sci.*, 2013, **4**, 310; (*c*) D. Ghosh and D. K. Mandal, *Fish Physiol. Biochem.*, 2014, **40**, 83.

19 (*a*) G. te Velde, F. M. Bickelhaupt, E. J. Baerends, C. Fonseca Guerra, S. J. A. van Gisbergen, J. G. Snijders and T. Ziegler, *J. Comput. Chem.*, 2001, **22**, 931 and references therein; (*b*) E. J. Baerends, J. Autschbach, D. Bashford, A. Bérces, F. M. Bickelhaupt,

C. Bo, P. M. Boerrigter, L. Cavallo, D. P. Chong, L. Deng, R. M. Dickson, D. E. Ellis, M. van Faassen, L. Fan, T. H. Fischer, C. Fonseca Guerra, A. Ghysels, A. Giammona, S. J. A. van Gisbergen, A. W. Götz, J. A. Groeneveld, O. V. Gritsenko, M. Grüning, F. E. Harris, P. van den Hoek, C. R. Jacob, H. Jacobsen, L. Jensen, G. van Kessel, F. Kootstra, M. V. Krykunov, E. van Lenthe, D. A. McCormack, A. Michalak, M. Mitoraj, J. Neugebauer, V. P. Nicu, L. Noodleman, V. P. Osinga, S. Patchkovskii, P. H. T. Philipsen, D. Post, C. C. Pye, W. Ravenek, J. I. Rodríguez, P. Ros, P. R. T. Schipper, G. Schreckenbach, M. Seth, J. G. Snijders, M. Solà, M. Swart, D. Swerhone, G. te Velde, P. Vernooijs, L. Versluis, L. Visscher, O. Visser, F. Wang, T. A. Wesolowski, E. M. van Wezenbeek, G. Wiesenekker, S. K. Wolff, T. K. Woo, A. L. Yakovlev and T. Ziegler, Theoretical Chemistry; Vrije Universiteit: Amsterdam.

20 (*a*) Copyright IBM Corp. 1990–2008, Copyright MPI für Festkörperforschung Stuttgart 1997–2001; (*b*) R. W. Hockney, *Meth. Comput. Phys.*, 1970, **9**, 136; (*c*) J. P. Perdew, K. Burke and M. Ernzerhof, *Phys. Rev. Lett.*, 1996, **77**, 3865; (*d*) W. Humphrey, A. Dalke and K. Schulten, *J. Molec. Graphics*, 1996, **14**, 33; (*d*) C. Hartwigsen, S. Goedecker and J. K. Hutter, *Phys. Rev. B*, 1998, **58**, 3641.

21 (*a*) J. VandeVondele and J. Hutter, *J. Chem. Phys.*, 2003, **118**, 4365; (*b*) M. Krack and M. Parrinello, *Forschungszentrum Jülich, NIC Series*, 2004, **25**, 29; (*d*) J. VandeVondele, M. Krack, F. Mohamed, M. Parrinello, T. Chassaing and J. Hutter, *Comput. Phys. Commun.*, 2005, **167**, 103.

22 M. J. Frisch, G. W. Trucks, H. B. Schlegel, G. E. Scuseria, M. A. Robb, J. R. Cheeseman, G. Scalmani, V. Barone, B. Mennucci, G. A. Petersson, H. Nakatsuji, M. Caricato, X. Li, H. P. Hratchian, A. F. Izmaylov, J. Bloino, G. Zheng, J. L. Sonnenberg, M. Hada, M. Ehara, K. Toyota, R. Fukuda, J. Hasegawa, M. Ishida, T. Nakajima, Y. Honda, O. Kitao, H. Nakai, T. Vreven, J. A. Montgomery Jr., J. E. Peralta, F. Ogliaro, M. Bearpark, J. J. Heyd, E. Brothers, K. N. Kudin, V. N. Staroverov, R. Kobayashi, J. Normand, K. Raghavachari, A. Rendell, J. C. Burant, S. S. Iyengar, J. Tomasi, M. Cossi, N. Rega, J. M. Millam, M. Klene, J. E. Knox, J. B. Cross, V. Bakken, C. Adamo, J. Jaramillo, R. Gomperts, R. E. Stratmann, O. Yazyev, A. J. Austin, R. Cammi, C. Pomelli, J. W. Ochterski, R. L. Martin, K. Morokuma, V. G. Zakrzewski, G. A. Voth, P. Salvador, J. J. Dannenberg, S. Dapprich, A. D. Daniels, Ö. Farkas, J. B. Foresman, J. V. Ortiz, J. Cioslowski and D. J. Fox, Gaussian 09, Gaussian Inc., Wallingford CT, 2009.

23 (*a*) E. R. Johnson, S. Keinan, P. Mori-Sánchez, J. Contreras-García, A. J. Cohen and W. Yang, *J. Am. Chem. Soc.*, 2010, **132**, 6498; (*b*) J. Contreras-García, E. R. Johnson, S. Keinan, R. Chaudret, J.-P. Piquemal, D. Beratan and W. Yang, *J. Chem. Theory Comput*., 2011, **7**, 625; (*c*) J. Contreras-García, W. Yang and E. R. Johnson, *J Phys Chem A*, 2011, **115**, 12983; (*d*) N. Gillet, R. Chaudret, J. Contreras-García, W. Yang, B. Silvi and J.-P. Piquemal *J. Chem. Theory Comput.*, 2012, **8**, 3993.

24 R. Kubin, *J. Lumin.*, 1983, **27**, 455.

25 E. Austin and M. Gouterman, *Bioinorg. Chem.*, 1978, **9**, 281.

26 G. L. Long and J. D. Winefordner, *Anal. Chem.*, 1983, **55**, 712A.

27 O. Visser, P. Leyronnas, W. J. van Zeist and M. Lupki, ADF-GUI 2012.01, SCM, Amsterdam, The Netherlands, http://www.scm.com.

28 (*a*) M. Mitoraj and A. Michalak, *J. Mol. Model.*, 2007, **13**, 347; (*b*) M. P. Mitoraj, A. Michalak and T. Ziegler, *J. Chem. Theory Comput.*, 2009, **5,** 962.

29 CrysAlisPro, Agilent Technologies, 2012, Version 1.171.36.21.

30 G. M. Sheldrick, *Acta Crystallogr.*, 2008, **A64**, 112.

31 I. J. Bruno, J. C. Cole, P. R. Edgington, M. Kessler, C. F. Macrae, P. McCabe, J. Pearson and R. Taylor, *Acta Crystallogr.*, 2002, **B58**, 389.